Hindawi
International Journal of Antennas and Propagation
Volume 2022, Article ID 6901105, 10 pages
https://doi.org/10.1155/2022/6901105

Research Article

Dynamic Characteristics Analysis and Applications of Electromagnetic Environment Based on Group Perception

Peiwei Gao,[1] **Yongfeng Zhi**,[1] **and Chufeng Hu**[2]

[1]*School of Automation, Northwestern Polytechnical University Department, Xi'an 710065, China*
[2]*Science and Technology on UAV Laboratory, Northwestern Polytechnical University, Xi'an 710065, China*

Correspondence should be addressed to Peiwei Gao; angelgao@nwpu.edu.cn

Received 18 January 2022; Revised 19 April 2022; Accepted 7 June 2022; Published 4 July 2022

Academic Editor: Angelo Liseno

In collectively perceiving an electromagnetic environment, the discrete or statistical method is used to characterize its characteristics. The information received by the sensor is not correlated with each other; therefore, there is no way to obtain the integral dynamic characteristics of an electromagnetic environment. Based on the statistical manifold and the information geometry theory, this paper takes group perception sensors in an electromagnetic space as an associated whole to measure an electromagnetic field in its space. The probability density function of the field distribution measured at any moment is mapped on to a statistical manifold. The "information distance" between the probability density functions of measurement samples at different moments of the statistical manifold is solved to reveal the changes in the whole electromagnetic environment. Simulations are carried out in assumed electromagnetic environments. The simulation results show that when a target enters the electromagnetic space and as its electromagnetic characteristics and positions change, the distribution of "*KLD* information distances" of its electromagnetic environment changes as well. The method can perceive the RCS of target with −26 dBsm and connect the target with its position information, indicating that the use of the "*KLD* information distance" distribution can characterize the integral dynamic characteristics of an electromagnetic environment.

1. Introduction

Carrying various sensors and working collectively in a coordinated way with ground monitoring stations, aerial platforms, and so on can ideally solve target detection problems in large key areas, thus burgeoning rapidly in recent years. In utilizing the group perception information of various sensors, the study of integral dynamic characteristics of the electromagnetic environment perceived by the sensors paves the way for solving the target detection problems in a complicated electromagnetic environment and provides a new way of thinking for the deep understanding, control, and utilization of electromagnetic environment characteristics.

Researchers have carried out massive analytical investigations of dynamic characteristics of the electromagnetic environment in terms of time, space, frequency, and energy [1–3]. However, in most cases, the discrete or statistical method is used to characterize the electromagnetic environment characteristics; the information received by various sensors is not correlated. Therefore, there is no way to obtain the integral dynamic characteristics of an electromagnetic environment. For example, Boksiner et al. studied the frequency spectral distribution of a battlefield electromagnetic environment [4]. Hippenstiel et al. used the nonlinear time-series statistical analysis to classify and characterize electromagnetic signals [5]. Jaekel used the phenomenon of electromagnetic environment to carry out its statistical description and classification [6]. Trigubovich described the statistical characteristics of an electromagnetic environment in its time domain, frequency domain, and energy domain [7]. Calin et al. used the experimental statistical method to study electromagnetic environments and analyzed the variations of the parameters of an electromagnetic field with time and space [8]. Nyah used the statistical model of certainty to analyze the electromagnetic environmental

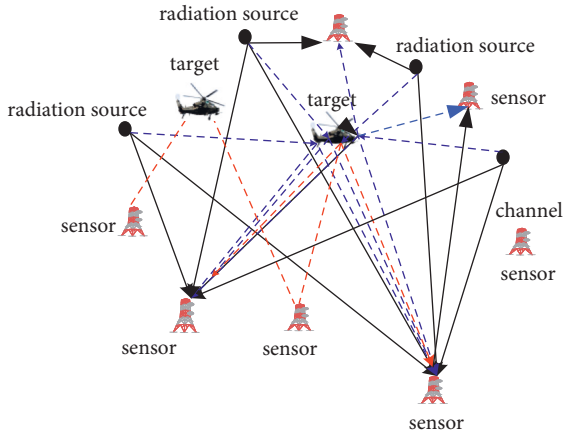

Figure 1: The electromagnetic environment characteristics group perception diagram.

parameters and their influence factors [9]. The studies that characterize the statistical fractal characteristics of the electromagnetic environment [10, 11] mainly used the discrete or statistical method to analyze its characteristics but did not reflect the connection between group perception and electromagnetic environmental information.

The existing solution is generally to analyze the field information of electromagnetic signal in discrete energy domain which is difficult to characterize the dynamic characteristics of the electromagnetic environment. Based on the sensor group perception characteristics and the information geometry theory, this paper takes the sensor group in an electromagnetic space as an associated whole to measure the distribution of an electromagnetic field in its space. The probability density function of the field distribution measured at any moment is mapped on to a statistical manifold. The "information distance" between the probability density functions of measurement samples at different moments of the statistical manifold is solved to reveal the changes in the whole electromagnetic environment. This paper provides a new solution to characterize the overall dynamic characteristics of electromagnetic environment.

2. Electromagnetic Environment Characteristics Group Perception Principles

The electromagnetic environment group perception diagram is shown in Figure 1.

The typical electromagnetic environment is made up of different types of electromagnetic radiation sources such as radio and television, wireless communications, and navigation signals. It carries out the group perception of its spatial characteristics through laying the sensor networks on the ground or in three-dimensional space, as shown in Figure 1. We assume that there are P number of electromagnetic radiation sources in a given region that the signal launched by a single radiation source is $S_p(t)$ and that the number of perception sensor network nodes is M. If the multipath signals of targets or surface features existing in an electromagnetic space are modeled as the contributions of a series of point scatterers, then the signals received by any node of the sensor network in the electromagnetic environment can be expressed as follows [12]:

$$R(t) = \sum_{p=1}^{P} A_p S_p\left(t - \tau_p\right) + \sum_{p=1}^{P}\sum_{n=1}^{Nc} C_{p,n} S_p\left(t - \Gamma_{p,n}^{c}\right) + \sum_{p=1}^{P}\sum_{m=1}^{Nt} \alpha_{p,m} S_p\left(t - \Gamma_{p,m}\right)\exp\left(j2\pi f_{p,m}^{D} t\right) + w(t). \tag{1}$$

In expression (1), the first item denotes the direct wave of each radiation source, the second item characterizes the surface feature multipath clutter signal, the third item is a target's echo-wave component, and the final item is noise. A_p and τ_p are direct wave attenuation and time-lag; $C_{p,n}$ and $\Gamma_{p,n}^{c}$ are clutter attenuation and time-lag; $\alpha_{p,m}$ and $\Gamma_{p,m}$ are the attenuation and time-lag of a target's echo-wave components; and $f_{p,m}^{D}$ is the Doppler frequency shift of the target's echo-wave. Therefore, in the group perception of the electromagnetic environmental shown in Figure 1, the electromagnetic environment signals collectively perceived by M number of sensor network nodes can be expressed as a set formed with signals received by M number of nodes as follows:

$$R = \{R_1, R_2, \ldots, R_M\}. \tag{2}$$

If the state distribution of the set R is X_k at the k moment and its state distribution is X_{k+1} at the $k+1$ moment, then the distribution of the "distance" between the state distributions X_{k+1} and X_k may characterize the dynamic characteristics of the electromagnetic environment measured by group perception sensor.

3. The Electromagnetic Environment Dynamic Characteristics Characterization Method Based on Information Geometry

3.1. Basic Principles of Information Geometry. Information geometry transforms into geometry the basic problems in probability theory and information theory studies as a whole a set of probability distribution function clusters and deeply mines the geometric structural information contained in them. Taking a typical normal distribution as an example, the normal distribution function cluster whose mean value is μ and whose co-variance is σ^2 as given in the following:

$$p(x;\mu,\sigma) = \frac{1}{\sqrt{2\pi}\sigma}\exp\left[-\frac{(x-\mu)^2}{2\sigma^2}\right]. \tag{3}$$

Figure 2 shows two groups of four normal distribution functions A, B, C, and D with different mean and standard deviation.

Figure 2 presents two groups of four normal distribution functions A, B, C, and D with different mean and standard deviation. Let $\mu_1 < \mu_2$ and $\sigma_1 < \sigma_2$ and consider the "difference" or distance between two probability distribution functions. Because the variance of A and B in Figure 2 is smaller than that of C and D, A and B are easier to separate

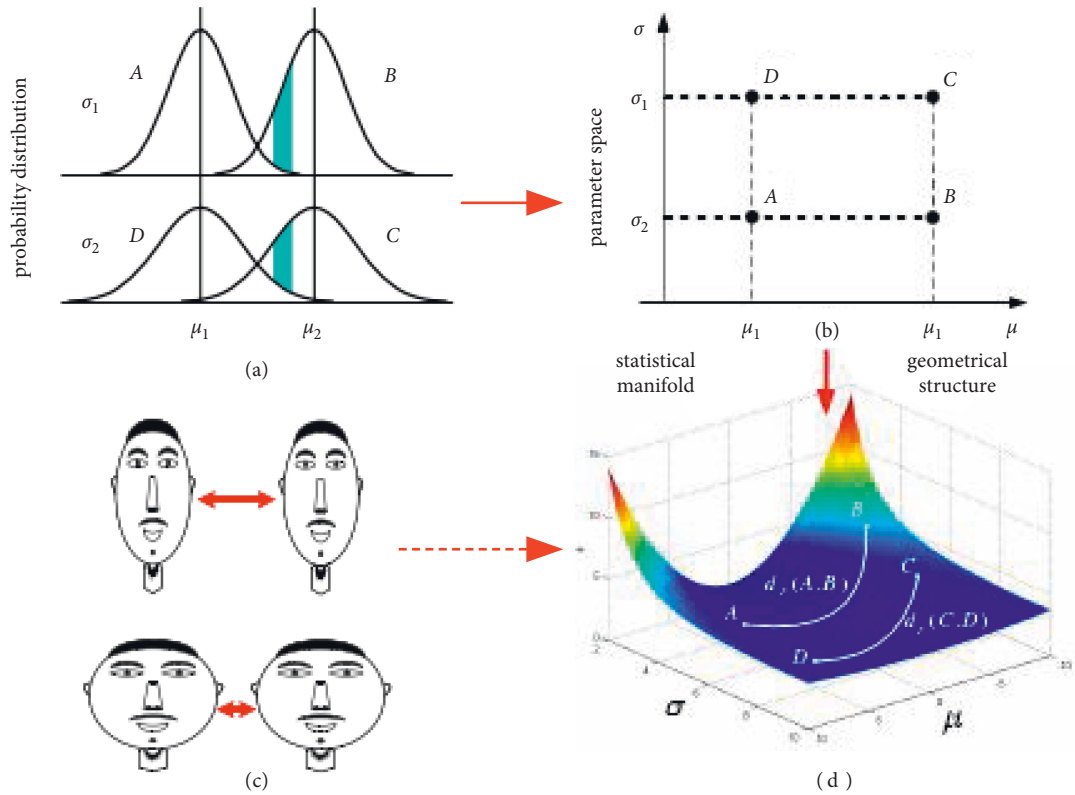

Figure 2: The transformation of probability space into geometry.

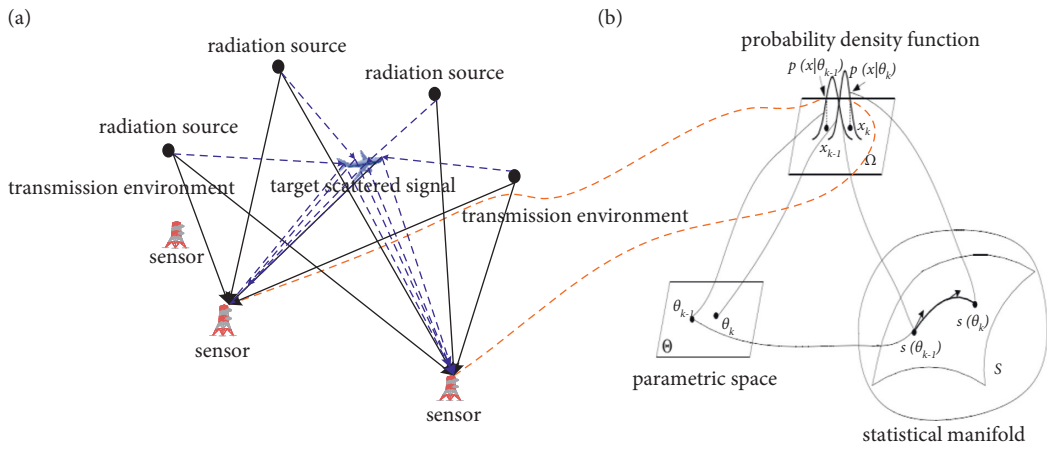

Figure 3: Mapping the sensor network measurement model to a statistical manifold. (a) Collective measurement model. (b) Statistical manifold.

than C and D; in other words, the distance between A and B is relatively farther. For fat man and thin man in Figure 2(c), the distance between thin man is relatively farther. If we use S to denote the above normal distribution function cluster, then its distribution parameters μ and σ can be expressed as four points in the parametric space P, as shown in Figure 2(b). Because $d(A, B) > d(C, D)$ (d denotes the distance between the two), the space corresponding to the normal distribution cluster S is a curved space and the curvature near A and B is larger than that near C and D. Such an abstract curved space is called the Riemann manifold [13]. The Riemann manifold formed with a probability distribution function cluster is also called statistical manifold, as shown in Figure 2(d). Every point on the statistical manifold corresponds to a probability distribution function.

The different type or different parameter probability distribution function cluster in Figure 2 corresponds to a statistical manifold that has a certain geometric structure. In the statistical manifold, the form of the probability distribution function decides the relationship between every probability distribution function and its adjacent ones, which decides the spatial structure formed by the

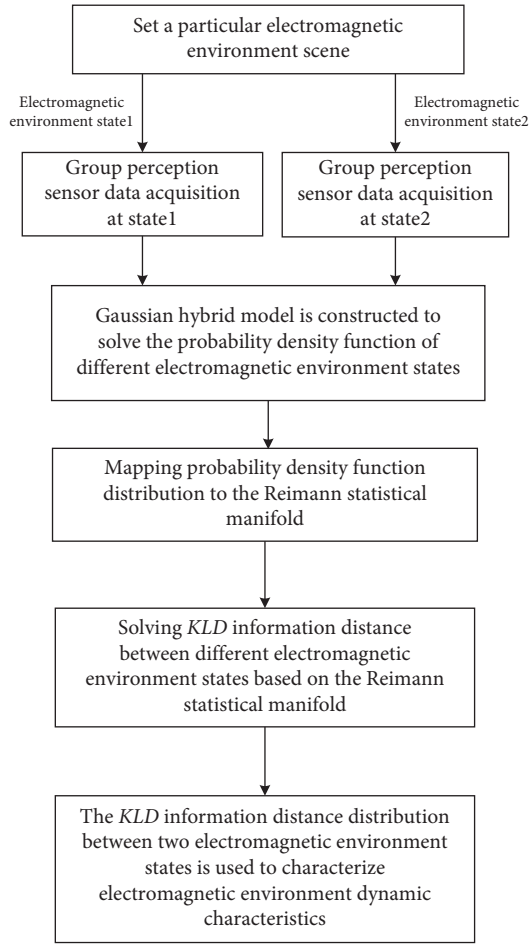

Figure 4: Algorithm procedural steps for electromagnetic environment dynamic characteristics.

relationship. Therefore, the geometric structure of a statistical manifold reveals the intrinsic essential attributes of the probability distribution function cluster. The prominent advantage of information geometry is that it studies the probability distribution function cluster as a set and uses a series of principles and methods to study the intrinsic structural information contained in the probability distribution.

3.2. The Electromagnetic Environment Dynamic Characteristics Characterization Based on Statistical Manifold. Based on the above analysis, with the help of the information geometry theory, the group perceived electromagnetic environment dynamic characteristics is characterized as follows.

3.2.1. Mapping the Sensor Network Measurement Model to a Statistical Manifold. In a given electromagnetic space, based on the information geometry principles, the collectively perceived sensor network is equalized to an entity and the probability density function cluster of its statistical model is mapped to a statistical manifold. Every random variable R_i in the set R sample set $R = \{R_1, R_2, \ldots, R_m\}$ formed with the sensor network measurement is mapped as a point in the statistical manifold, as shown in Figure 3. Therefore, the use of states of points on the statistical manifold at any moment, namely, the distribution of probability density function clusters, can characterize the electromagnetic environment state distribution measured by the sensor network perceived collectively at this moment. At a certain moment when there are new targets, electromagnetic threats, or factors that may influence the change in their states, the electromagnetic environment state distribution, thus measured will have "perturbation," namely, the state distribution will change relative to the previous moment. This perturbation may be mapped as the changes in information distance between two groups of probability density function clusters on the statistical manifold.

In Figure 3(b), Ω is the group perception sensors measurement sample space, whose probability density function is $p(x|\theta)$; θ is the parameter vector of $p(x|\theta)$; Θ is the vector space of the parameter θ; S is the statistical manifold that uses the parameter θ as its coordinates and can be expressed as follows:

$$S = \left\{ p\left(\frac{x}{\theta}\right) \middle| \theta \in \Theta \subseteq \mathbb{R}^n \right\}, \tag{4}$$

where x is any measurement sample in an electromagnetic space. $x \in \Omega \subseteq \mathbb{R}^m$, x is the sample of the random variable R that has M number of dimensions. Figure 3(b) reveals the relationship among the parameter θ, the measurement sample x, and the statistical manifold. In this way, the probability density function distribution of the sample x measured at any moment can be used to characterize the electromagnetic environment state perceived collectively at the moment.

Furthermore, in order to solve the changes in characteristics among different electromagnetic environment states, the integral distance between any two points $p(x|\theta_1)$ and $p(x|\theta_1)$ curve on the statistical manifold in Figure 3(b) is as follows [14]:

$$D(\theta_1, \theta_2) \triangleq \int_{t_1}^{t_2} \sqrt{\left(\frac{\mathrm{d}\theta}{\mathrm{d}t}\right)^T G(\theta) \left(\frac{\mathrm{d}\theta}{\mathrm{d}t}\right)} \mathrm{d}t. \tag{5}$$

The integral distance in equation (5) depends on the selection of the curve $p(x|\theta_1)$ that connects the two points; its minimum length is the Fisher information distance and can be expressed as follows [15]:

$$D_F(\theta_1, \theta_2) \triangleq \min_{\theta(t)} \int_{t_1}^{t_2} \sqrt{\left(\frac{\mathrm{d}\theta}{\mathrm{d}t}\right)^T G(\theta) \left(\frac{\mathrm{d}\theta}{\mathrm{d}t}\right)} \mathrm{d}t. \tag{6}$$

Except for some special manifolds, generally it is rather difficult to directly calculate the Fisher information distance in equation (6). Therefore, the information distance between the two probability distributions $p(x|\theta_1)$ and $p(x|\theta_2)$ can be approximated with other measurement methods. The most widely used method is the Kullback–Leibler divergence degree, which can be expressed as follows:

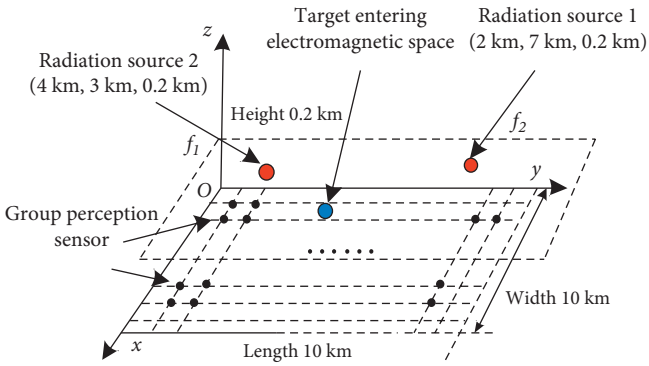

Figure 5: The simulation scene.

$$KLD[p(x|\theta_1)\|p(x|\theta_2)] = \int p(x|\theta_1)\ln\frac{p(x|\theta_1)}{p(x|\theta_2)}\mathrm{d}x. \quad (7)$$

Thus, each probability density function distribution on the statistical manifold, namely, the information distance distribution, can be used to characterize the dynamic characteristics of the collectively perceived electromagnetic environment.

3.2.2. Solving Dynamic Characteristics of a Collectively Perceived Electromagnetic Environment. Based on the above analysis, the following algorithm procedural steps can be used to solve the electromagnetic environment dynamic characteristics, as shown in Figure 4:

In Figure 4, for a particular electromagnetic environment scene, we use the space-time synchronous group perception sensor to sample and measure massive data. A certain amount of measurement data is accumulated and then preprocessed. Based on the measurement sample, we use the Gaussian hybrid model as the probability density function model to be solved and then map the probability density function distribution of the measurement sample to a statistical manifold to characterize the electromagnetic environment state during the acquisition. Finally, we solve the *KLD* information distance among the probability density function distributions of different electromagnetic environment states to characterize their dynamic characteristics. The key to the algorithm procedural steps lies in the probability density function solution and the *KLD* information distance calculation.

To solve the probability density function of a measurement sample, we use the limited Gaussian hybrid algorithm to fit and solve the Gaussian hybrid model. Hershey and Olsen have proved that the finite Gaussian hybrid algorithm can approximate arbitrary probability distribution with any precision. Given that the random variable x obeys the Gaussian hybrid distribution, its distribution function can be defined as follows [16]:

$$f(x) = \sum_{i=1}^{k}\lambda_i N_i\left(x;\mu_i,\sigma_i^2\right), \quad (8)$$

where k is the number of the Gaussian component; $N_i(x;\mu_i,\sigma_i^2)$ is the *ith* Gaussian component; λ_i is the hybrid weighted coefficient of the *ith* Gaussian component; and the parameter set of the model is $\theta = \{\lambda_i,\mu_i,\sigma_i^2\}$. We fit the parameters in a parameter set with measurement samples, thus approximating different probability distributions. In actual applications, the use of the finite Gaussian hybrid model for fitting complicated probability distributions requires an equilibrium point between the model's number of orders and fitting accuracy.

To solve the *KLD* information distance, we assume that two given Gaussian hybrid distribution functions are as follows:

$$\begin{aligned} f(x) &= \sum_{i=1}^{Ns}\alpha_i f_i(x),\\ g(x) &= \sum_{j=1}^{Nm}\beta_j g_j(x), \end{aligned} \quad (9)$$

where $f_i(x)$ and $g_i(x)$ are the Gaussian distributions, whose mean values are, respectively, μ_i and ν_i, and whose co-variances are, respectively, σ^2 and γ^2; Ns and Nm are, respectively, numbers of components of the two models; and α_i and β_i are the hybrid weighted values of the number of components. According to equation (7), the information distance between $f(x)$ and $g(x)$ can be expressed as follows:

$$KLD[f(x)\|g(x)]^{def} = \int f(x)\log\frac{f(x)}{g(x)}\mathrm{d}x. \quad (10)$$

Definition:

$$\begin{aligned} L_f(f) &= E_{f(x)}[\log f(x)],\\ L_f(g) &= E_{f(x)}[\log g(x)]. \end{aligned} \quad (11)$$

Therefore, the *KLD* information distance can be further expressed as follows:

$$\begin{aligned} KLD[f(x)\|g(x)] &= E_{f(x)}[\log f(x)] - E_{f((x))}[\log g(x)]\\ &= L_f(f) - L_f(g). \end{aligned} \quad (12)$$

The use of the Jensen in equation produces:

$$\begin{aligned} L_f(g) = E_{f(x)}[\log g(x)] &= \sum_i \alpha_i E_{f_i(x)}\left[\log\left(\sum_j \beta_j g_j(x)\right)\right]\\ &\le \sum_i \alpha_i \log\left\{\sum_j \beta_j E_{f_i(x)}\left[g_j(x)\right]\right\}\\ &= \sum_i \alpha_i \log\left[\sum_j \beta_j \int f_i(x) g_j(x)\mathrm{d}x\right]. \end{aligned} \quad (13)$$

Then,

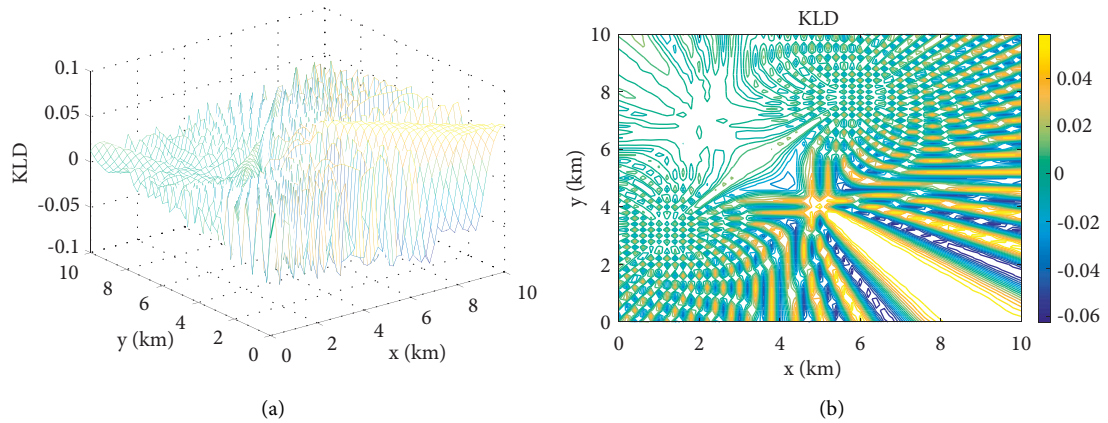

FIGURE 6: The simulation results when the target's RCS is 0 dBsm. (a) The 3D *KLD* information distance distribution. (b) The 2D *KLD* information distance distribution.

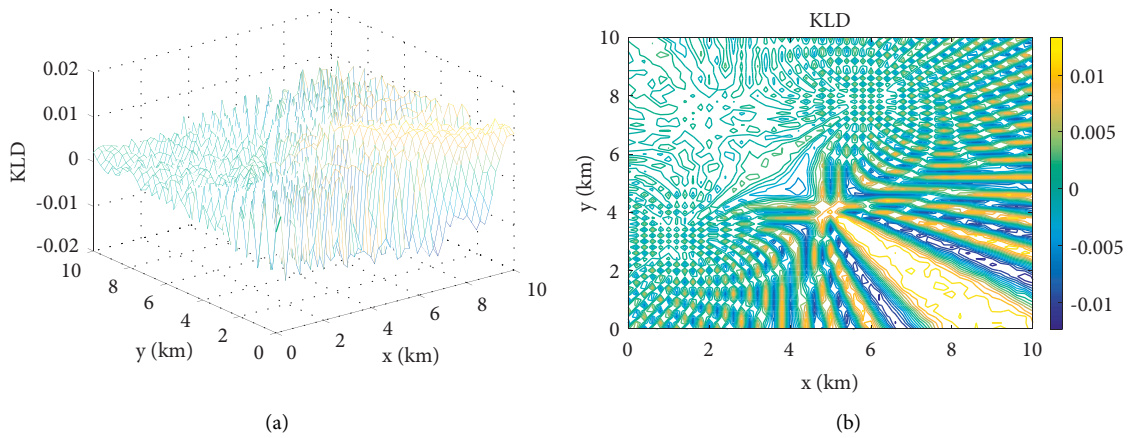

FIGURE 7: The simulation results when the target's RCS is −20 dBsm. (a) The 3D *KLD* information distance distribution. (b) The 2D *KLD* information distance distribution.

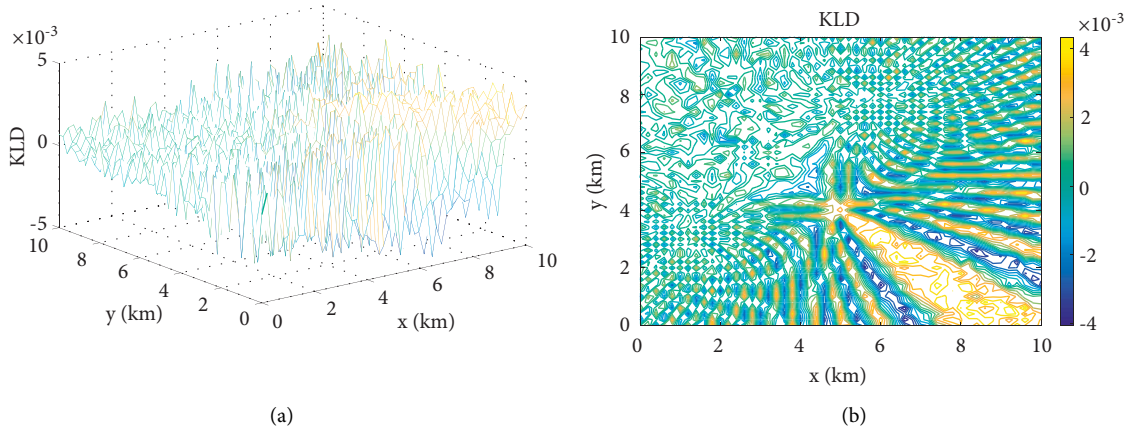

FIGURE 8: The simulation results when the target's RCS is −26 dBsm. (a) The 3D *KLD* information distance distribution. (b) The 2D *KLD* information distance distribution.

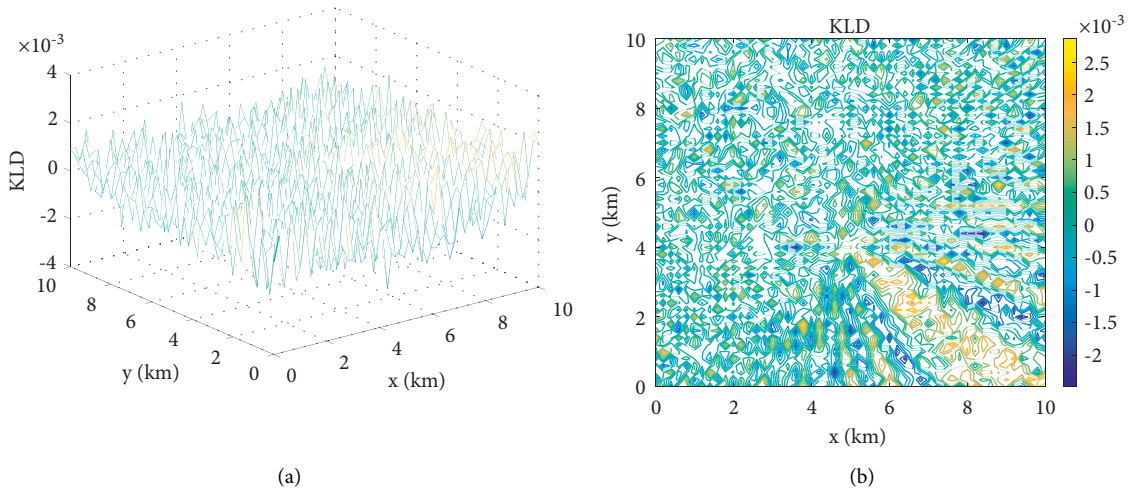

(a) (b)

Figure 9: The simulation results when the target's RCS is −40 dBsm. (a) The 3D *KLD* information distance distribution. (b) The 2D *KLD* information distance distribution.

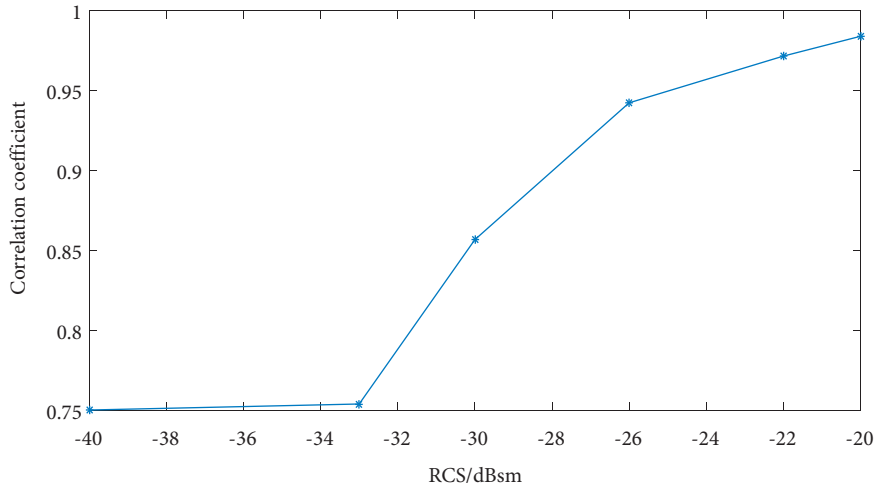

Figure 10: The correlation coefficient between the KLD information distance matrix of different RCS values and the reference matrix.

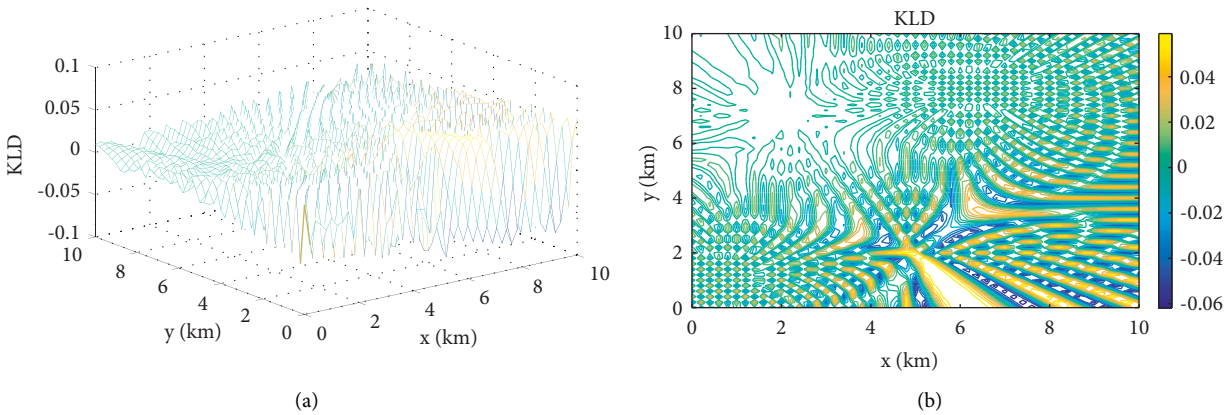

(a) (b)

Figure 11: The simulation results when a target appears at Position *A*. (a) The 3D *KLD* information distance distribution. (b) The 2D *KLD* information distance distribution.

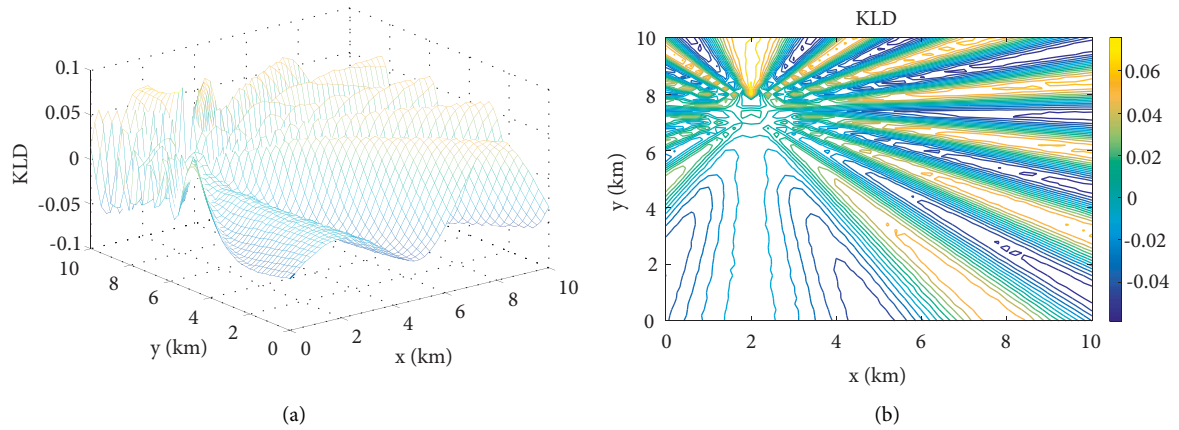

(a) (b)

Figure 12: The simulation results when a target appears at Position *B*. (a) The 3D *KLD* information distance distribution. (b) The 2D *KLD* information distance distribution.

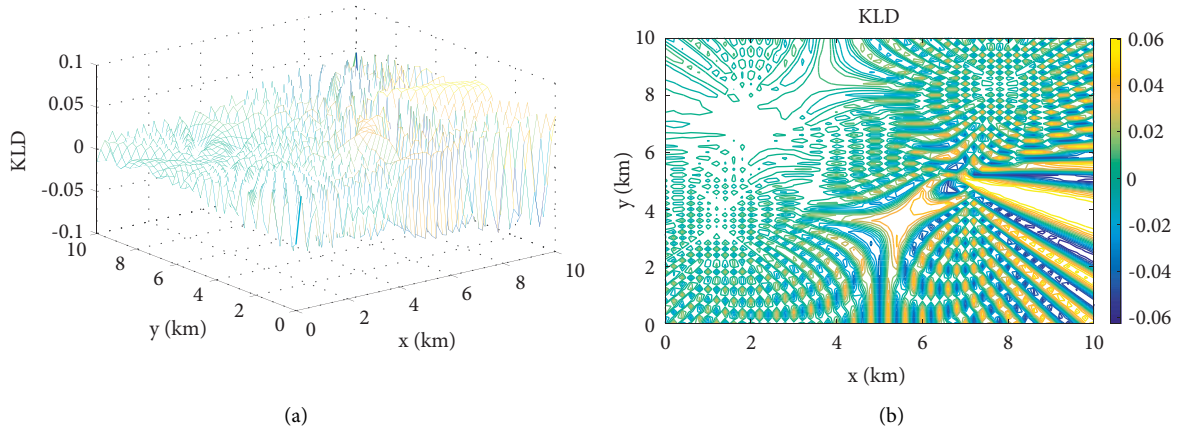

(a) (b)

Figure 13: The simulation results when a target appears at Position *C*. (a) The 3D *KLD* information distance distribution. (b) The 2D *KLD* information distance distribution.

$$L_f(g) \le \sum_i \alpha_i \log\left[\sum_j \beta_j \int f_i(x) g_j(x) \mathrm{d}x\right] = \sum_i \alpha_i \log\left(\sum_j \beta_i z_{ij}\right), \quad (14)$$

where $z_{ij} \triangleq \int f_i(x) g_j(x) \mathrm{d}x$. The approximate analytic values of the *KLD* information distance between $f(x)$ and $g(x)$ can be expressed as follows:

$$KLD(f(x) \| g(x)) = \sum_i \alpha_i \log\left(\sum_{i'} \alpha_i z_{ii'} / \sum_j \beta_j z_{ij}\right), \quad (15)$$

where $z_{ii'} \triangleq \int f_i(x) f_{i'}(x) \mathrm{d}x$. With the above derivations, the approximate analytic values of the *KLD* information distance we can be calculated.

4. The Simulation Results

4.1. Simulation Conditions. For simulation, we assume that the electromagnetic environment measurement range is 10 km long, 10 km wide, and 0.2 km high. The environment has two radiation sources whose modulation mode are BPSK and FSK, respectively. The transmission power is set as 5 kW, and the central frequency points are $f_1 = 900$ MHz and $f_2 = 90$ MHz, respectively. The model of signal propagation is free space propagation model. Given that the group perception sensor for measurement is laid out and has the interval of 200 m, the simulation scene is shown in Figure 5.

When a new target appears in the above simulation scene and has different electromagnetic characteristics or different positions, we simulate and analyze the changes in dynamic characteristics of the group perception electromagnetic environment.

4.2. Simulating Different Electromagnetic Characteristics of the Target. Assuming that the new target is a point target and that its coordinate space is (5 km, 4 km, and 0.02 km), when its Radar Cross Section (RCS) scattering characteristics are 0 dBsm, −20 dBsm, −26 dBsm, and −40 dBsm, the simulation results on the dynamic characteristics of the collectively perceived electromagnetic environment are shown in Figures 6–9.

Figures 6–9 show that when the RCS of the electromagnetic target is 0 dBsm, the *KLD* information distance between the electromagnetic environment states when a target is present or absent is from −0.06 to 0.04. When the RCS is −20 dBsm, the distribution of *KLD* information distance is from −0.01 to 0.01. When the RCS is −26 dBsm, the distribution of *KLD* information distance is from −0.004 to 0.004. When the RCS is −40 dBsm, the distribution of *KLD* information distance is from −0.002 to 0.0025. In this simulation scene, when the RCS of the target that enters an electromagnetic environment dwindles, the *KLD* information distance distribution magnitude also dwindles. In the above set electromagnetic environment scene, when the target's RCS is 0 dBsm, −20 dBsm, or −26 dBsm, its *KLD* information distance distribution has an obvious connection with its position. When the target's RCS is −40 dBsm, its *KLD* information distance distribution has no connection with its position information. Taking the KLD information distance matrix with the target RCS of 0dBsm as the reference matrix, when the target RCS is −20 dBsm, −22 dBsm, −26 dBsm, −30 dBsm, −33 dBsm, and −40 dBsm, respectively, the correlation coefficient between the KLD information distance matrix of different RCS values and the reference matrix is solved, and the results are shown in Figure 10.

According to Figure 10, when the correlation coefficient is greater than 0.9 (0.9 is a threshold for detection), the *KLD* information distance distribution can perceive the target whose smallest RCS is −26 dBsm.

4.3. The Simulation and Analysis of a Target in Different Positions. Supposing that a target enters simulation scene, that the RCS of the electromagnetic target is 0dBsm, and that it appears, respectively, at positions A (5 km, 2 km, and 0.01 km), B (2 km, 8 km, and 0.01 km), and C (7 km, 5 km, and 0.01 km), the simulation results on the dynamic characteristics of the collectively perceived electromagnetic environment are given in Figures 11–13.

Figures 11–13 show that when an electromagnetic target appears at different positions, the *KLD* information distance distribution of electromagnetic environment states between the presence and absence of the target is obviously different. The *KLD* information distance distribution is closely related to the position of the target and ranges from −0.06 to 0.04.

The above simulation results show that in the set electromagnetic environment scene, when a new target enters it, the situation of the electromagnetic environment will change, and the change is related to the scattering characteristics and position of the target entering the electromagnetic space. Hence, based on group perception sensor measurement information, the *KLD* information distance distribution can be used to characterize the integral dynamic characteristics of the electromagnetic environment on the statistical manifold.

5. Conclusions

The study of the integral dynamic characteristics of an electromagnetic environment is the basis for its understanding, control, and utilization. With the help of the information geometry theory, this paper equalizes the group perception sensor network as an entity. The information distance distribution is used to describe the integral dynamic characteristics of the electromagnetic environment. Furthermore, because the dynamic characteristics of electromagnetic environment characterized with the information distance distribution are closely related to the characteristics and position of a target entering the electromagnetic space. The electromagnetic environment integral characteristics information can be further used to carry out target detection. In the future, the influence on the dynamic characteristics of the electromagnetic environment with different target RCS will be measured and verified in the anechoic chamber.

The proposed method may be applied to actual applications of physical platforms in the future, such as artificial lateral line detection system of underwater robot [17]. The artificial lateral line detection array is used to collect information of underwater environment, and the flow field distribution of underwater environment can be measured, then the position of target in the environment can be detected. On the other hand, it can also be used to optimize the layout and quantity of artificial lateral line detection array and improve the accuracy of target position detection.

Data Availability

No data were used to support this study.

Conflicts of Interest

The authors declare that they have no conflicts of interest.

Acknowledgments

This work was supported by the Research Projects (07B003, 07B001) and the National Natural Science Foundation of China (61571368).

References

[1] G. Chmaj and H. Selvaraj, "Distributed processing applications for UAV/drones: a survey," in *Proceedings of the Progress in Systems Engineering*, pp. 449–454, Las Vegas, NV, U.S.A, August 2015.

[2] L. Li, T. Wang, and Q. L. Hu, "White force network in DARPA CODE program," *Aerospace Electron Warfare*, vol. 34, no. 06, pp. 54–59, 2018.

[3] L. Gupta, R. Jain, and G. Vaszkun, "Survey of important issues in UAV communication networks," *IEEE Communications Surveys and Tutorials*, vol. 18, pp. 1123–1152, 2015.

[4] J. Boksiner, Y. Posherstnik, B. May, M. Saltzman, and S. Kamal, "Centrally controlled dynamic spectrum access for manets," in *Proceedings of the MILCOM 2013-IEEE Military Communications Conference*, pp. 641–646, San Diego, CA, U.S.A, November 2013.

[5] R. Hippenstiel, H. E. Kishky, and P. Radev, "On time-series analysis and signal classification-part I: fractal dimensions," in *Proceedings of the Conference on Signals, Systems & Computers IEEE*, pp. 2121–2125, Pacific Grove, CA, U.S.A, November 2004.

[6] B. W. Jaekel, "Approaches for description of electromagnetic environments and compatibility levels," in *Proceedings of the International Symposium and Exhibition on Electromagnetic Compatibility and Electromagnetic Ecology*, pp. 176–182, St. Petersburg, Russia, May 2009.

[7] W. B. Trigubovich, "On some characteristics of electromagnetic environment," in *Proceedings of the International Conference on Mathematical Methods in Electromagnetic Theory*, pp. 191–196, Kharkov, Ukraine, June 1998.

[8] M. D. Calin, C. Ursachi, and E. Helerea, "Electromagnetic environment characteristics in an urban area," *Electrical Engineering and Applied Physics*, vol. 11, no. 1, pp. 117–124, 2013.

[9] C. T. Nyah, "Developing a statistical model for electromagnetic environment for mobile wireless networks," *World Academy of Science, Engineering and Technology*, vol. 6, no. 1, pp. 617–620, 2012.

[10] J. Yang, B. M. Bian, and Z. G. Yan, "Fractal characteristics of characteristic parameter statistical distributions of typical random signals," *Acta Physica Sinica*, vol. 60, no. 10, pp. 1–7, 2011.

[11] J. Dong, X. Y. Pu, H. Han, and L. N. Hong, "Fractal characteristics and quantification method of electromagnetic environment," *Journal of Terahertz Science and Electronic Information Technology*, vol. 12, no. 3, pp. 428–432, 2014.

[12] J. Yi, X. Wan, H. Leung, and F. Cheng, "MIMO passive radar tracking under a single frequency network," *IEEE Journal of Selected Topics in Signal Processing*, vol. 9, no. 8, pp. 1661–1671, 2015.

[13] F. Opitz, *Information Geometry and its Applications*Springer Publishing Company, Tokyo, 2016.

[14] S. Costa, S. A. Santos, and J. E. Strapasson, "Fisher information matrix and hyperbolic geometry," in *Proceedings of the IEEE ISOC ITW 2005 On Coding and Complexity*, pp. 34–36, Rotorua, New Zealand, August 2005.

[15] W. Li and Y. Jia, "Kullback-Leibler divergence for interacting multi-model estimation with random matrices," *IET Signal Processing*, vol. 10, no. 1, pp. 12–18, 2015.

[16] J. R. Hershey and P. A. Olsen, "Approximating the Kullback leibler divergence between Gaussian mixture models," in *Proceedings of the 2007 IEEE International Conference on Acoustics, Speech and Signal Processing - ICASSP*, vol. 07, pp. 317–320, Honolulu, HI, U.S.A, April 2007.

[17] X. Zheng, W. Wang, L. Li, and G. M. Xie, "Artificial lateral line based relative state estimation between an upstream oscillating fin and a downstream robotic fish," *Bioinspiration & Biomimetics*, vol. 16, Article ID 016012, 2021.